ADVANCED MATERIALS
www.advmat.de

Magnetic Plasmon Networks Programmed by Molecular Self-Assembly

Pengfei Wang, Ji-Hyeok Huh, Jaewon Lee, Kwangjin Kim, Kyung Jin Park, Seungwoo Lee,* and Yonggang Ke**

Nanoscale manipulation of magnetic fields has been a long-term pursuit in plasmonics and metamaterials, as it can enable a range of appealing optical properties, such as high-sensitivity circular dichroism, directional scattering, and low-refractive-index materials. Inspired by the natural magnetism of aromatic molecules, the cyclic ring cluster of plasmonic nanoparticles (NPs) has been suggested as a promising architecture with induced unnatural magnetism, especially at visible frequencies. However, it remains challenging to assemble plasmonic NPs into complex networks exhibiting strong visible magnetism. Here, a DNA-origami-based strategy is introduced to realize molecular self-assembly of NPs forming complex magnetic architectures, exhibiting emergent properties including anti-ferromagnetism, purely magnetic-based Fano resonances, and magnetic surface plasmon polaritons. The basic building block, a gold NP (AuNP) ring consisting of six AuNP seeds, is arranged on a DNA origami frame with nanometer precision. The subsequent hierarchical assembly of the AuNP rings leads to the formation of higher-order networks of clusters and polymeric chains. Strong emergent plasmonic properties are induced by in situ growth of silver upon the AuNP seeds. This work may facilitate the development of a tunable and scalable DNA-based strategy for the assembly of optical magnetic circuitry, as well as plasmonic metamaterials with high fidelity.

Manipulation of magnetic fields at nanoscale can enable a range of new optical properties including high-sensitivity circular dichroism,[1] directional scattering,[2] and low refractive index.[3] Natural aromatic molecules (e.g., benzene, naphthalene, chrysene, and triphenylene) exhibit a ring current of delocalized π-electrons under an external magnetic field, which is perpendicularly aligned with respect to the plane of the ring. The circulating displacement current, consequently, induces a local magnetic field according to Ampère law (referred to as magnetism). Such molecular-scale magnetism may be artificially realized at optical frequencies by using aromatic molecule-inspired cyclic ring cluster of metallic nanoparticles (NPs), herein referred to as optical magnetic ring.[3e,4,5] Like their molecular counterparts, the near-field coupling between the metallic NPs in the cyclic ring can produce a circular current caused by electron displacement, when illuminated with an external electromagnetic field. Furthermore, bridging these artificial optical magnetic rings into complex and scalable networks ranging from supracolloidal clusters to linear chains enables coupling and traveling of magnetic plasmons with significantly reduced loss, providing a potent platform for controlling light–matter interaction with unprecedented degree of freedom.

The vast majority of such architectures with artificial optical magnetisms so far were fabricated with electron-beam (e-beam) lithography.[6] However, the accessible structural sizes with this method are relatively large (i.e., a few hundred nanometers for NP size and a few nanometers for gap size), which limits their application at higher frequencies. Moreover, the serial fabrication process has hindered its capability in organizing magnetic rings to form complex networks with emergent properties; as such, it is exclusively used for the fabrication of discrete unit of magnetic rings.[6,7]

Prof. P. Wang
Institute of Molecular Medicine (IMM)
Renji Hospital
Shanghai Jiao Tong University School of Medicine
Shanghai 200127, China
E-mail: pengfei.wang@sjtu.edu.cn

J.-H. Huh, J. Lee, K. Kim, K. J. Park, Prof. S. Lee
KU-KIST Graduate School of Converging Science and Technology
Korea University
Seoul 02841, Republic of Korea
E-mail: seungwoo@korea.ac.kr

The ORCID identification number(s) for the author(s) of this article can be found under https://doi.org/10.1002/adma.201901364.

Prof. S. Lee
Department of Biomicrosystem Technology
Korea University
Seoul 02841, Republic of Korea

Prof. Y. Ke
Wallace H. Coulter Department of Biomedical Engineering
Georgia Institute of Technology and Emory University
Atlanta, GA 30322, USA
E-mail: yonggang.ke@emory.edu

Prof. Y. Ke
Department of Chemistry
Emory University
Atlanta, GA 30322, USA

DOI: 10.1002/adma.201901364

Alternatively, the bottom-up assembly of colloidal NPs has been often used to assemble optical magnetic rings composed of smaller NPs, from an initial demonstration of raspberry-like clustering metallic NPs to the recent demonstration of feedback-controlled assembly of gold nanorod dimer.[4b–d,8] These colloidal self-assembly strategies, however, also face the challenge of bridging magnetic rings in a scalable manner to form higher-order clusters or networks, because they are mainly governed by the nonprogrammable packing mechanism.[4c,8h]

Structural DNA nanotechnology[9] provides a promising platform toward complex architectures of NP optical magnetic rings, as it has demonstrated unparalleled capability for the deterministic assembly of metallic NPs with nanometer precision.[10] Here, by using programmable assembly of DNA origami,[9c,e,f,10f] we established a three-step fabrication procedure to generate optical magnetic rings, clusters, and 1D chains composing of NPs with emergent optical properties (**Scheme 1**). We first used a DNA origami hexagon tile (DHT)[10a] to precisely assemble six AuNPs (10 nm in diameter) into a monocyclic ring structure. Then, subsequent hierarchical assembly of the tile led to higher-order networks ranging from bicyclic, tricyclic, tetracyclic, to 1D chain of cyclic rings. At last, these structures were deposited onto a flat substrate and followed by in situ silver growth to enlarge NPs and to enhance the plasmonic coupling while preserving structural complexity and integrity.[10e,f,11] Emergent properties of magnetic plasmons such as anti-ferromagnetism, a purely magnetic Fano resonance, and magnetic surface plasmon polaritons (SPPs) were successfully realized.

We first systematically examined how the electric and magnetic dipolar (ED and MD) resonances vary according to the number of silver NPs (AgNP) in the cyclic ring by using numerical calculation (**Figure 1**a,b). Symmetric geometry was employed in the calculation to avoid asymmetric axis-enabled side effects such as Fano resonance.[4c,6a] The size of AgNPs and nanogap was designated as 45 nm and 1 nm, respectively, based on our experimental measurements. Derivations and decompositions of multipolar moments, which have been the standard for the analyses of plasmonic metamolecules,[4–6] were employed to quantify the contributions of ED and MD to the total resonant behaviors. More critically, the macroscopic constitutive parameters including effective permittivity, permeability, and refractive index can be directly correlated with such microscopic ED and MD moments by using effective medium theory (i.e., the Maxwell–Garnett (M–G) relation).[4a] Thus, the numerical calculations and experimental analyses of microscopic ED/MD are essential for envisioning prospects of our optical magnetic rings.

The calculation revealed that an increase in AgNP number from 3 (trimer) to 6 (hexamer) enhances both ED and MD resonances together with red-shifting of resonance peak positions (Figure 1a). Noticeably, the ED and MD resonances of the hexamer-based cyclic ring were found to be sufficiently strong to induce unnatural negative refractive index (Figure 1b), and the required volume of this cyclic ring for achieving negative

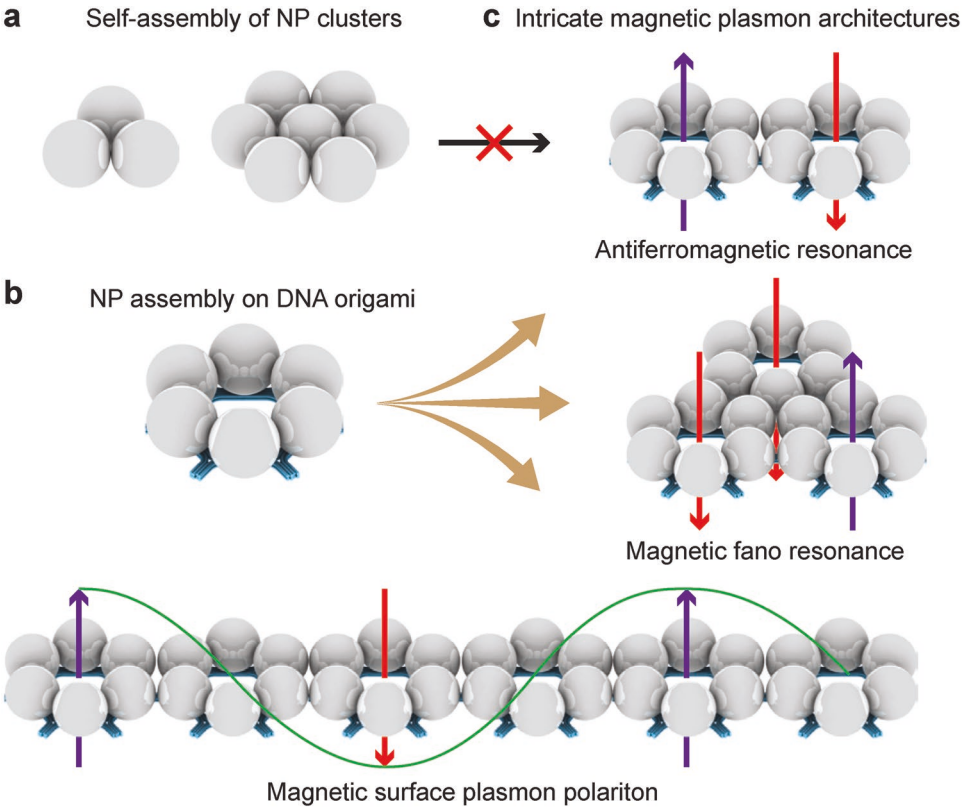

Scheme 1. Complex magnetic plasmon nanoparticle networks assembled on DNA templates. a) Conventional nanoparticle assembly produces relatively simple, closely packed clusters. b) A hexagon NP ring assembled on DNA origami. c) Programmable assembly of DNA origami leads to intricate magnetic plasmon architectures, including magnetic surface plasmon polariton.

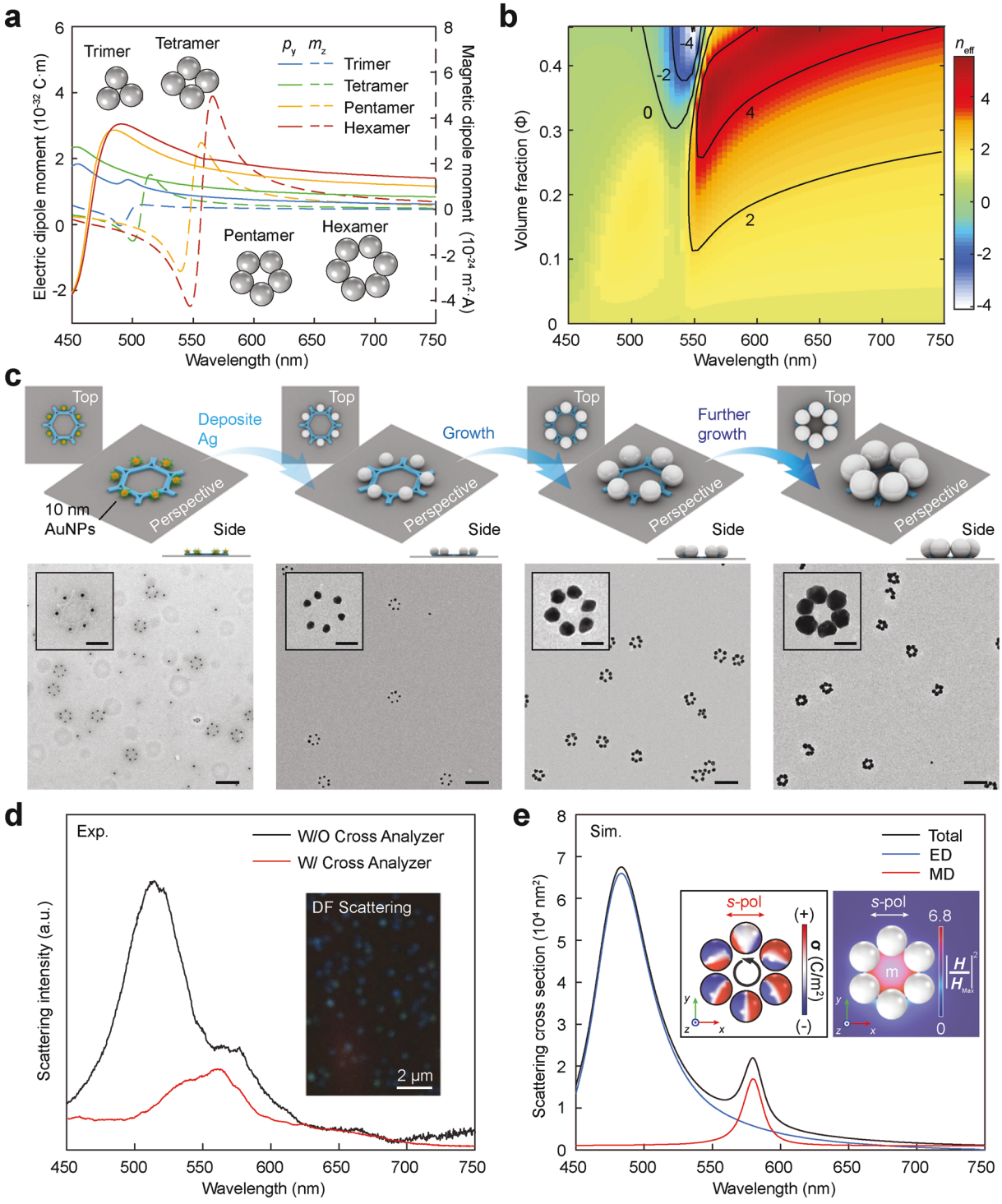

Figure 1. Construction of magnetic rings. a) Theoretical analysis of electric (p_y) and magnetic (m_z) dipole moments, accessible with magnetic rings composed of 3 (trimer), 4 (tetramer), 5 (pentamer), and 6 (hexamer) silver (Ag) nanoparticles (NPs). Herein, 45 nm sized AgNPs were assumed to be closely packed into clusters with 1 nm gap. b) Effective refractive index of optical effective medium composing of AgNPs hexamer (the main motif of magnetic ring, used in this study) as function of volume fraction. Effective medium theory, based on Maxwell–Garnett relation, was used to obtain effective refraction index. c) Schematics and TEM images of magnetic rings, which were constructed via stepwise growth of AgNPs. Scale bars: 200 nm, 50 nm (insets). d) Dark-field (DF) scattering spectra of the self-assembled magnetic ring (AgNP hexamer) together with corresponding DF optical microscopy image. e) Scattering cross-section (SCS) of optical magnetic ring, which was calculated by finite element method. Electric and magnetic dipolar (ED and MD) contributions to total SCS were separately highlighted and accumulated to obtain total SCS. The spatial distributions of surface charge density (σ, C m^{-2}) and the induced magnetic field intensity (normalized to the maximal amplitude of the incident one) are included in the inset of (e).

refractive index at the visible regimes is smaller than that of other counterparts reported so far (≈30 vol% at the resonance wavelength (≈540 nm)).[8c] The corresponding magnetic susceptibility (χ) is included in Figure S1 in the Supporting Information. As such, we chose our DHT motif with six exterior binding sites for anchoring NPs as a template to self-assemble the hexamer-based cyclic ring (Figure S2 in the Supporting Information shows caDNAno design of the DHT). Further increase in AgNP number, for example, heptamer, may induce other complex resonances including Fano resonance, which could reduce the ED and MD resonance strength.[4c]

The magnetic ring was successfully fabricated as illustrated in Figure 1c. Six 10 nm AuNPs were first anchored onto the exterior sides of the DHT frame with high yield of ≈90% (Figure S3, Supporting Information). The monocyclic magnetic ring was then fully developed by growing silver on this precursor ring of AuNPs, which was first deposited onto a flat substrate of copper grid. The size of AgNPs was tailored via adjusting the growth time. To induce strong electric coupling, the AgNP size was tuned to be between 40 and 45 nm and the interparticle gap is within a few nanometers, as measured from transmission electron microscopy (TEM) images. The on-surface silver growth appeared critical for the fabrication of magnetic rings with high fidelity. The initial surface deposition of rings with small AuNP seeds alleviates deposition-caused structural distortion, which is commonly observed in solution-based growth. The ring geometry was well preserved and the center-to-center interparticle distance showed neglectable change after on-surface silver growth (Figure S4, Supporting Information).

In agreement with our calculation results, the assembled monocyclic ring exhibited a strong magnetism (Figure 1d,e). Dark-field (DF) scattering colors were consistent across the assembled monocyclic rings (Figure 1d, inset). More critically, the representative DF scattering peak and shoulder at 500 and 570 nm wavelengths (Figure 1d, dark line) resulted respectively from the ED and MD resonances. A set of DF scattering spectra across the assembled magnetic rings (approximately ten samples) with varied structural uniformity was collected (Figure S5, Supporting Information). Despite their structural irregularities, characteristic features of ED and MD remained across different samples, indicating that magnetic rings are quite tolerant to structural imperfections. Cross analyzer, located at scattering pathway, selectively elucidated MD response (red line in Figure 1d) via screening ED counterpart. Herein, *s*-polarized and slanted (64°) light was used to couple the vertical component of the incident magnetic field with the plane of a magnetic ring. These experimental results matched well with theoretical spectra (scattering cross-section (SCS)), calculated with 45 nm AgNPs and 1 nm gap (Figure 1e), confirming the high structural fidelity of the assembled monocyclic magnetic ring. In this work, the Au nanoseed was excluded for numerical calculations, since it has negligible influence on the resonant features (see Figure S6 in the Supporting Information). The surface charge density (σ) and the induced MD distribution at 570 nm wavelength are included in insets of Figure 1e. The circulating displacement electric field at MD resonance wavelength, resulting from near-field coupling between AgNPs, further evidenced the artificial magnetism, whereas ED resonant characteristics were highlighted by a linear-like dipolar oscillation of charges, as shown in Figure S7 in the Supporting Information. These modal analyses imply that both ED and MD modes are driven by the induced movement of the charge along the whole AgNPs in monocyclic ring rather than local gap or AgNP. This resonant feature, in turn, makes both ED and MD modes robust to the structural imperfections, once the ring geometry is well maintained (Figure S5, Supporting Information).

Taking advantage of the programmable intermolecular interaction between DHTs, bicyclic (**Figure 2**a), tricyclic (Figure 2b), tetracyclic (Figure 2c), and 1D chain (Figure 2d) of magnetic rings were fabricated by the hierarchical assembly of monocyclic ring precursors, followed by on-surface silver growth (see Figures S8–S20 in the Supporting Information for more information). It is noteworthy that such scalable and higher-order assembly of plasmonic NPs into closely packed clusters and chains exhibited sufficiently high quality, which would be difficult to achieve from direct self-assembly of large metallic NPs (>30 nm) on DNA origami due to strong steric hindrance and electrostatic repulsion between large NPs.

The programmable assembly of magnetic rings resulted in interesting emergent magnetic properties. The bicyclic magnetic ring composing of 40 nm AgNPs and 5 nm gap exhibited an anti-ferromagnetic coupling between the induced magnetic fields within each ring (**Figure 3**a,c). When incoming electric field is polarized along a short axis of bicyclic magnetic ring (*s*-pol), circulating displacement current along each cyclic ring can occur in opposite direction with each other (at wavelength of 560 nm, noted as resonance 2); consequently, MD within bicyclic magnetic ring can be resonantly induced in anti-ferromagnetic fashion (Figure 3a). This anti-ferromagnetic circulating displacement current is contrasted with in-phase ED oscillations at wavelength of 455 nm (Figure S21, Supporting Information). As the radiations driven by such induced MD oscillations within each ring can be constructively interfered, this anti-ferromagnetic resonance is a super-radiant mode (also called bright mode). Thereby, we observed a distinct DF scattering peak from the self-assembled bicyclic ring at 560 nm wavelength (Figure 3b). The DF scattering peak at 460 nm wavelength originated from ED oscillation. In addition to this representative spectrum, DF scattering spectral variations across the assembled bicyclic rings are summarized in Figure S22 in the Supporting Information, showing a relative uniformity of ED/MD resonances. Using cross analyzer allowed for the selective reduction of the ED resonant contribution to scattering spectra as with monocyclic magnetic ring. Thereby, anti-ferromagnetic scattering becomes more visible (red line in Figure 3b). This DF scattering spectra showed a good agreement with theoretical SCS spectra (Figure 3c). A slight shoulder in DF scattering spectra was observed at 530 nm wavelength in contrast to the theoretical prediction. This was derived from the partial mixing of *p*-pol component of incident light in a real experiment, as detailed in Figure S23 in the Supporting Information.

Higher-order clusters of cyclic ring networks such as tricyclic and tetracyclic magnetic rings were found to conceive more complex coupling of magnetic plasmons (Figure 3d–f; Figures S24 and S25, Supporting Information). As shown in numerical simulation, tricyclic magnetic ring networks can meet the condition of a purely magnetic Fano resonance, resulting from strong near-field coupling. When illuminated

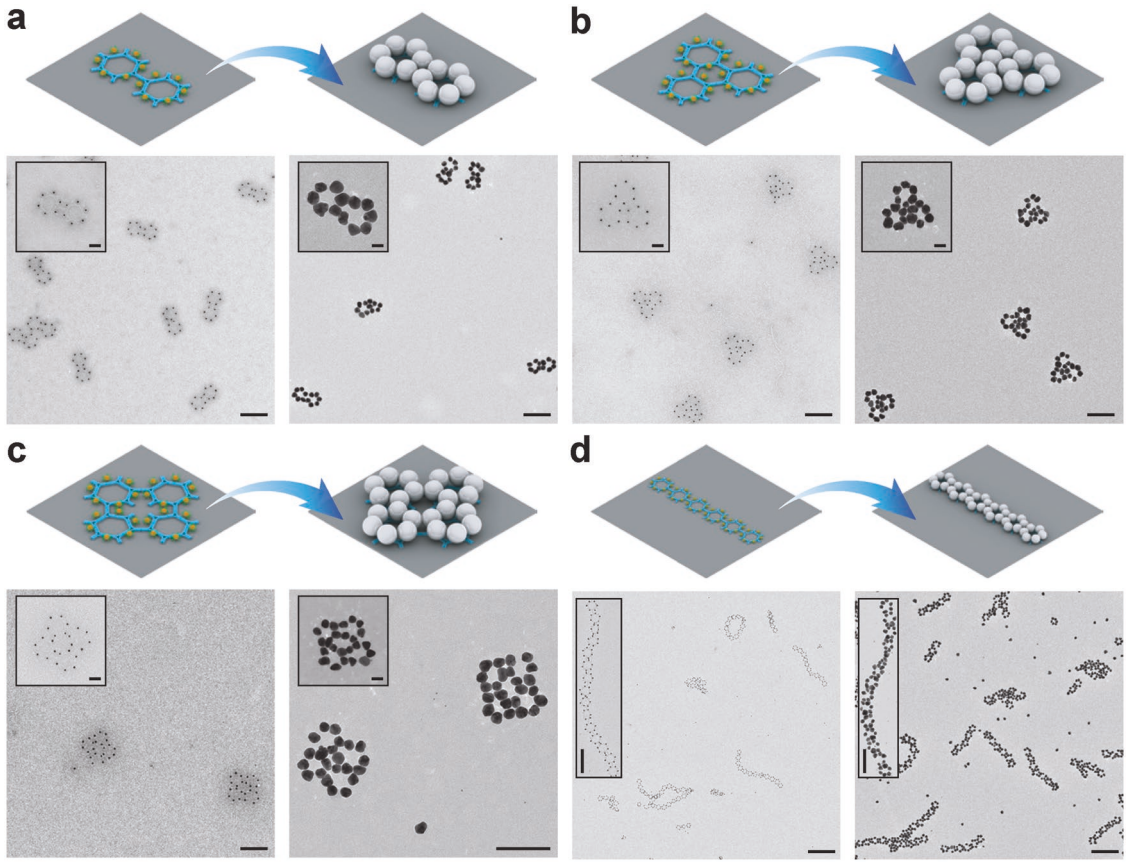

Figure 2. a–d) Structural evolutions for: a) bicyclic, b) tricyclic, c) tetracyclic, and d) 1D chain networks of magnetic rings. Scale bars, a–c): 200 nm, 50 nm (insets); d): 500 nm, 200 nm (insets).

with *s*-pol, tricyclic magnetic ring networks consisting of 40 nm AgNP and 5 nm gap can induce MD resonances within each ring (resonance 2). In this mode, the displacement currents in rings 1 and 2 are circulated along the same direction; but, opposite with respect to that in ring 3 (top panel of Figure 3d). The radiations from these MD resonances were found to constructively interfere, so as to result in a distinct DF scattering peak at resonance 2 (bright mode), as shown in Figure 3e. This observation of the bright radiation from MD resonances matched well with the theoretical SCS spectra (Figure 3f). Corresponding DF scattering spectral variations across the tricyclic rings (see Figure S26 in the Supporting Information) confirm the robustness of their ED/MD resonances to a structural imperfection.

At wavelength of 575 nm, the energy for the MD resonance was partially transferred to excite another circulating displacement current within a small ring inclusion between ring 1, 2, and 3 (bottom panel of Figure 3d). This energy storage, in turn, induced Fano resonant dip in DF scattering spectra at 575 nm (subradiant magnetic resonance, named as resonance 1). The spatial distributions of the induced magnetic field at the wavelengths of the resonance 1 and 2 are shown in Figure S24 in the Supporting Information. Such purely magnetic Fano resonance was achieved via a strong near-field coupling between the rings. For example, when three rings are sufficiently separated from each other, the induced MDs cannot be effectively coupled, as evidenced by a single shoulder of SCS at a shorter wavelength compared with that of resonance 1 (Figure S25, Supporting Information). This Fano resonant DF scattering dip also showed a good agreement with the theoretical SCS spectra (Figure 3f). It is noteworthy that the position of the absorption cross-section (ACS) peak matched with that of SCS dip, further confirming that the resonant energy is stored via a purely magnetic Fano resonance. Meanwhile, tetracyclic magnetic ring showed the Fano coupling between the broad electric and narrow magnetic resonances; these results are detailed in Figure S27 in the Supporting Information.

Finally, we aimed to propagate magnetic plasmons along the linear 1D chain, as shown in **Figure 4**. DNA origami has been suggested as a promising template for fabricating 1D chains of NPs.[10e,f,12] Recently, DNA origami has been used to organize plasmonic NPs into 1D chains exhibiting waveguide function.[13] In particular, ED resonance can be cascaded along the individual plasmonic NPs arrayed in 1D chain. However, the practical use of such propagation of electric plasmons is largely compromised due to their strong optical loss. In contrast, optical loss can be dramatically reduced by magnetic plasmonic propagation, by which the resonant circular displacement current can be propagated (i.e., magnetic surface plasmon polaritons).[7a] In particular, the induced magnetic field can excite the anti-ferromagnetic propagation. Consequently, optical loss caused by intrinsic absorption of metals or

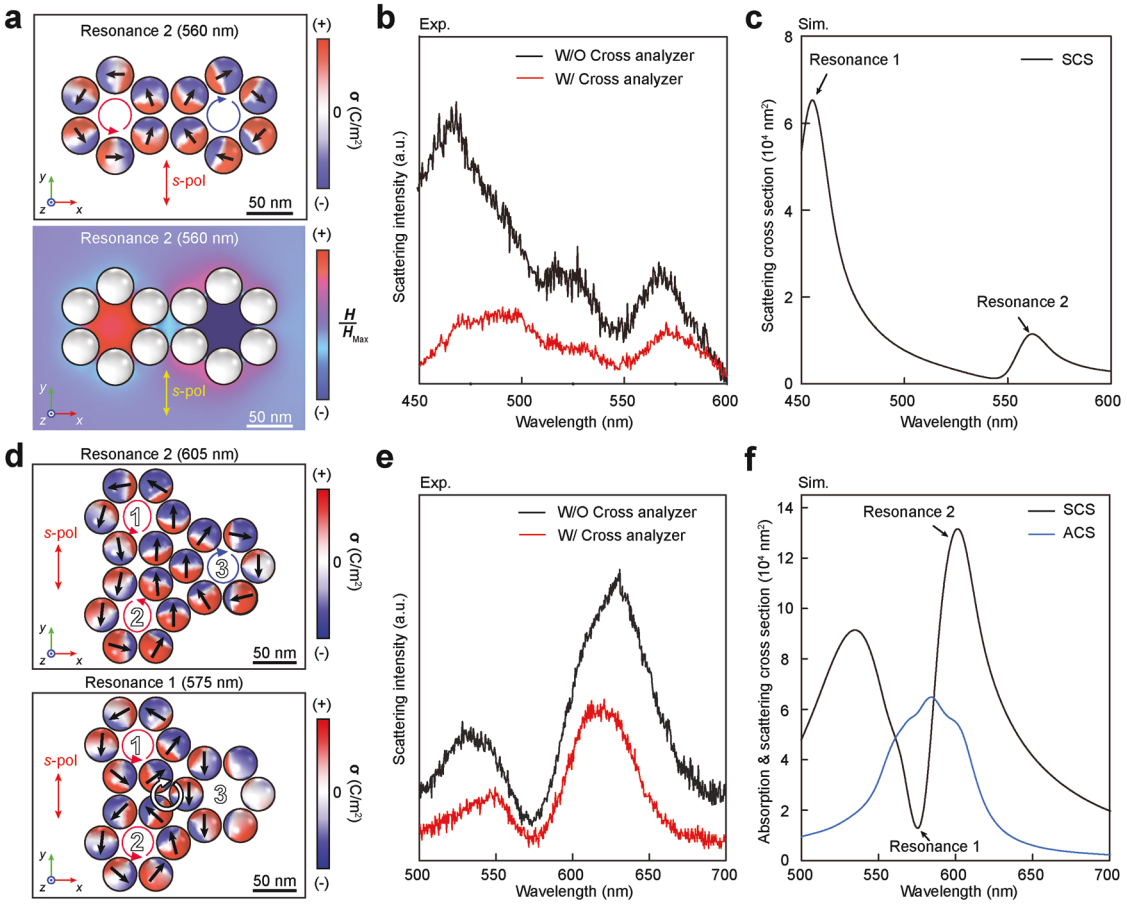

Figure 3. Bicyclic and tricyclic magnetic rings. a) The spatial distributions of σ (top panel) and the induced magnetic field magnitude, normalized to the maximal amplitude of the incident one (bottom panel) at the anti-ferromagnetic resonant mode of bicyclic magnetic rings (noted by resonance 2). b) DF scattering spectra of bicyclic magnetic rings. c) SCS of bicyclic magnetic rings. d) The spatial distributions of σ of tricyclic magnetic rings at the MD resonance (resonance 2 at 605 nm wavelength) and a purely magnetic Fano resonance (resonance 1 at 575 nm wavelength). e) DF scattering spectra of tricyclic magnetic rings. f) SCS and absorption cross-section (ACS) of tricyclic magnetic rings.

structural defects can be mitigated. Nevertheless, the magnetic SPPs have not been experimentally reported so far possibly due to the challenges in fabrication.

Our 1D chain of cyclic rings was found able to excite magnetic SPPs. Figure 4 illustrates the optical characterization results of magnetic SPPs from a 1D chain comprising of six cyclic rings. TEM image of the 1D chain was shown in Figure 4a (40 nm AgNP and 5 nm gap in average). Herein, the multiple SPP modes, which were mixed with electric and magnetic SPPs, were simultaneously excited. As such, various DF scattering colors were observed (Figure 4b). The corresponding DF scattering spectrum obtained without cross analyzer (black line in Figure 4c) showed a good match with theoretical SCS spectra (Figure 4d) excepting a scattering intensity at resonance 1 (520 nm wavelength). The DF scattering intensity ratio of resonance 1 to resonance 2 (660 nm wavelength) was lower than the theoretical prediction. Note that the resonance 1 corresponds to the ED-based electric SPPs (Figure S28, Supporting Information), while magnetic SPPs give an origin of resonance 2 (Figure 4e,f). Particularly, the MD confined along the subset of three rings was found to propagate in anti-ferromagnetic fashion and form a standing wave along a 1D chain of rings. The insertion of cross analyzer further confirmed the magnetic SPP-based radiation of resonance 2 (red line of Figure 4c). This result implies that magnetic SPPs can be more robust than ED counterparts against optical loss caused by a realistic experimental condition (e.g., irregularity of AgNP shape and size). To the best of our knowledge, this is the first observation of magnetic SPPs in experimental circumstances. The scattering peak at 575 nm originated from an ED, which was driven by the partially impinged *p*-pol component of incident light (Figure S29, Supporting Information). An increase in number of magnetic rings in 1D chain did not notably change the resonance position and modal characteristics of magnetic SPPs, as shown in Figure S30 in the Supporting Information; as such, a routing of a long-lived magnetic SPP could be also accessible with our synthetic method. Overall, this DNA-origami-based programmable self-assembly can be generalized to control over the coupling and propagating of magnetic plasmons.

In conclusion, our work provides a general platform for scalable networking of magnetic plasmons, in which DNA origami was used as a template for the guided assembly and seed growth of plasmonic NPs. A stepwise approach enables

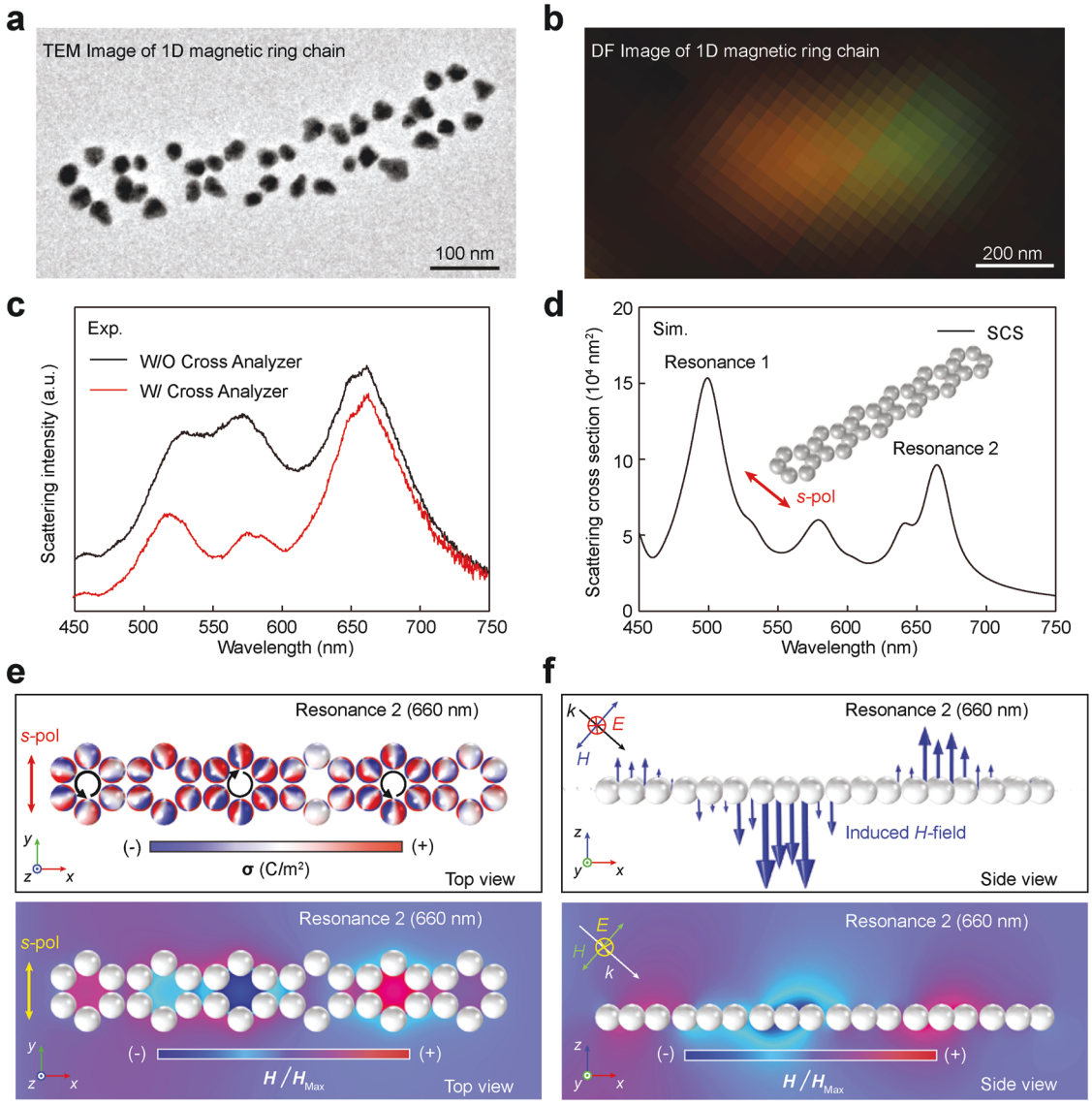

Figure 4. 1D chain of magnetic rings. a) TEM image and b) DF optical microscopy image of a 1D chain composing of six magnetic rings. c) The corresponding DF scattering spectra. d) The numerically simulated SCS of 1D chain. The modal analysis of magnetic SPPs of 1D chain at the wavelength of 660 nm (resonance 2). e) The top-view spatial distributions of σ (top panel) and the induced magnetic field magnitude, normalized to the maximal amplitude of the incident one (bottom panel); and f) the side-view spatial distributions of the induced magnetic field (top panel) and magnitude (bottom panel), normalized to the maximal amplitude of the incident one.

the scalable assembly of higher-order networks of plasmonic NPs with high fidelity. In contrast to conventional colloidal self-assembly,[4c,8h] DNA-origami-templated seed-growth method is fully modularized and molecularly programmable. Thus, highly sophisticated networks of NP rings can be fabricated. In addition to mono-, bi-, tri-, tetra-, and linear-cyclic ring clusters demonstrated here, more delicate networks exhibiting fascinating metamaterial properties may be realized through evolving assembly pathways (e.g., algorithmic assembly) in future. Looking forward, we envision that molecular self-assembly route may lead to the manufacture of optical metamaterials with unprecedented nanostructural complexity and associated electromagnetic properties, in a high-throughput, parallel process.

Supporting Information

Supporting Information is available from the Wiley Online Library or from the author.

Acknowledgements

P.W. and J.H. contributed equally to this work. This work was supported by the National Research Foundation of Korea (NRF of Korea) Project 2017M3D1A1039421 and 2016R1D1A1B03930454, the KU-KIST School Project, the KU startup fund program (K1824561) to S.L., and an NSF grant ECCS-1807568 to Y.K. P.W. thanks the startup support from the Institute of Molecular Medicine, Shanghai Jiao Tong University School of Medicine. Some EM data was gathered on the Hitachi HT7700 120 kV TEM supported by the Atlanta Clinical and Translational Science Institute (ACTSI) award UL1TR000454.

Conflict of Interest

The authors declare no conflict of interest.

Keywords

artificial magnetism, colloids, DNA nanotechnology, plasmonics, self-assembly

Received: February 28, 2019
Revised: April 23, 2019
Published online:

[1] a) H. Z. Zhiyuan Fan, A. O. Govorov, *J. Phys. Chem. C* **2013**, *117*, 14770; b) S. Yoo, Q. H. Park, *Phys. Rev. Lett.* **2015**, *114*, 203003; c) Y. Tang, A. E. Cohen, *Phys. Rev. Lett.* **2010**, *104*, 163901; d) A. García-Etxarri, J. A. Dionne, *Phys. Rev. B* **2013**, *87*, 235409.

[2] a) A. I. Kuznetsov, A. E. Miroshnichenko, Y. H. Fu, J. Zhang, B. Luk'yanchuk, *Sci. Rep.* **2012**, *2*, 492; b) Y. H. Fu, A. I. Kuznetsov, A. E. Miroshnichenko, Y. F. Yu, B. Luk'yanchuk, *Nat. Commun.* **2013**, *4*, 1527.

[3] a) A. Atre, A. Garcia, H. Alaeian, J. Dionne, *Adv. Opt. Mater.* **2013**, *1*, 327; b) R. A. Shelby, D. R. Smith, S. Schultz, *Science* **2001**, *292*, 77; c) C. Enkrich, M. Wegener, S. Linden, S. Burger, L. Zschiedrich, F. Schmidt, J. F. Zhou, T. Koschny, C. M. Soukoulis, *Phys. Rev. Lett.* **2005**, *95*, 203901; d) A. K. Sarychev, G. Shvets, V. M. Shalaev, *Phys. Rev. E: Stat., Nonlinear, Soft Matter Phys.* **2006**, *73*, 036609; e) Y. A. Urzhumov, G. Shvets, J. A. Fan, F. Capasso, D. Brandl, P. Nordlander, *Opt. Express* **2007**, *15*, 14129; f) I. Liberal, N. Engheta, *Science* **2017**, *358*, 1540; g) J. Valentine, S. Zhang, T. Zentgraf, E. Ulin-Avila, D. A. Genov, G. Bartal, X. Zhang, *Nature* **2008**, *455*, 376.

[4] a) S. Y. Kwangjin Kim, J.-H. Huh, Q.-H. Park, S. Lee, *ACS Photonics* **2017**, *4*, 2298; b) Z. Qian, S. P. Hastings, C. Li, B. Edward, C. K. McGinn, N. Engheta, Z. Fakhraai, S. J. Park, *ACS Nano* **2015**, *9*, 1263; c) J. A. Fan, C. H. Wu, K. Bao, J. M. Bao, R. Bardhan, N. J. Halas, V. N. Manoharan, P. Nordlander, G. Shvets, F. Capasso, *Science* **2010**, *328*, 1135; d) A. S. Urban, X. Shen, Y. Wang, N. Large, H. Wang, M. W. Knight, P. Nordlander, H. Chen, N. J. Halas, *Nano Lett.* **2013**, *13*, 4399.

[5] A. Alu, A. Salandrino, *Opt. Express* **2006**, *14*, 1557.

[6] a) N. Verellen, Y. Sonnefraud, H. Sobhani, F. Hao, V. V. Moshchalkov, P. Van Dorpe, P. Nordlander, S. A. Maier, *Nano Lett.* **2009**, *9*, 1663; b) T. Han, S. Zu, Z. Li, M. Jiang, X. Zhu, Z. Fang, *Nano Lett.* **2018**, *18*, 567; c) D. E. Gomez, Z. Q. Teo, M. Altissimo, T. J. Davis, S. Earl, A. Roberts, *Nano Lett.* **2013**, *13*, 3722; d) Y. Bao, Z. Hu, Z. Li, X. Zhu, Z. Fang, *Small* **2015**, *11*, 2177.

[7] a) N. Liu, S. Mukherjee, K. Bao, Y. Li, L. V. Brown, P. Nordlander, N. J. Halas, *ACS Nano* **2012**, *6*, 5482; b) N. Liu, S. Mukherjee, K. Bao, L. V. Brown, J. Dorfmuller, P. Nordlander, N. J. Halas, *Nano Lett.* **2012**, *12*, 364.

[8] a) S. Yang, X. Ni, X. Yin, B. Kante, P. Zhang, J. Zhu, Y. Wang, X. Zhang, *Nat. Nanotechnol.* **2014**, *9*, 1002; b) J. Shi, F. Monticone, S. Elias, Y. Wu, D. Ratchford, X. Li, A. Alu, *Nat. Commun.* **2014**, *5*, 3896; c) S. N. Sheikholeslami, H. Alaeian, A. L. Koh, J. A. Dionne, *Nano Lett.* **2013**, *13*, 4137; d) F. Shafiei, F. Monticone, K. Q. Le, X. X. Liu, T. Hartsfield, A. Alu, X. Li, *Nat. Nanotechnol.* **2013**, *8*, 95; e) K. J. Park, J. H. Huh, D. W. Jung, J. S. Park, G. H. Choi, G. Lee, P. J. Yoo, H. G. Park, G. R. Yi, S. Lee, *Sci. Rep.* **2017**, *7*, 6045; f) S. Muhlig, C. Rockstuhl, V. Yannopapas, T. Burgi, N. Shalkevich, F. Lederer, *Opt. Express* **2011**, *19*, 9607; g) S. Muhlig, A. Cunningham, S. Scheeler, C. Pacholski, T. Burgi, C. Rockstuhl, F. Lederer, *ACS Nano* **2011**, *5*, 6586; h) J. A. Fan, K. Bao, C. Wu, J. Bao, R. Bardhan, N. J. Halas, V. N. Manoharan, G. Shvets, P. Nordlander, F. Capasso, *Nano Lett.* **2010**, *10*, 4680.

[9] a) P. F. Wang, T. A. Meyer, V. Pan, P. K. Dutta, Y. G. Ke, *Chem* **2017**, *2*, 359; b) N. C. Seeman, H. F. Sleiman, *Nat. Rev. Mater.* **2017**, *3*, 1; c) P. W. K. Rothemund, *Nature* **2006**, *440*, 297; d) F. Hong, F. Zhang, Y. Liu, H. Yan, *Chem. Rev.* **2017**, *117*, 12584; e) S. M. Douglas, H. Dietz, T. Liedl, B. Hogberg, F. Graf, W. M. Shih, *Nature* **2009**, *459*, 1154; f) H. Dietz, S. M. Douglas, W. M. Shih, *Science* **2009**, *325*, 725.

[10] a) P. F. Wang, S. Gaitanaros, S. Lee, M. Bathe, W. M. Shih, Y. G. Ke, *J. Am. Chem. Soc.* **2016**, *138*, 7733; b) M. J. Urban, P. K. Dutta, P. F. Wang, X. Y. Duan, X. B. Shen, B. Q. Ding, Y. G. Ke, N. Liu, *J. Am. Chem. Soc.* **2016**, *138*, 5495; c) Y. Tian, T. Wang, W. Y. Liu, H. L. Xin, H. L. Li, Y. G. Ke, W. M. Shih, O. Gang, *Nat. Nanotechnol.* **2015**, *10*, 637; d) E. M. Roller, L. K. Khorashad, M. Fedoruk, R. Schreiber, A. O. Govorov, T. Liedl, *Nano Lett.* **2015**, *15*, 1368; e) M. Pilo-Pais, S. Goldberg, E. Samano, T. H. LaBean, G. Finkelstein, *Nano Lett.* **2011**, *11*, 3489; f) A. Kuzyk, R. Schreiber, Z. Y. Fan, G. Pardatscher, E. M. Roller, A. Hogele, F. C. Simmel, A. O. Govorov, T. Liedl, *Nature* **2012**, *483*, 311.

[11] W. Sun, E. Boulais, Y. Hakobyan, W. L. Wang, A. Guan, M. Bathe, P. Yin, *Science* **2014**, *346*, 1258361.

[12] X. Lan, T. Liu, Z. Wang, A. O. Govorov, H. Yan, Y. Liu, *J. Am. Chem. Soc.* **2018**, *140*, 11763.

[13] F. N. Gur, C. P. T. McPolin, S. Raza, M. Mayer, D. J. Roth, A. M. Steiner, M. Loffler, A. Fery, M. L. Brongersma, A. V. Zayats, T. A. F. Konig, T. L. Schmidt, *Nano Lett.* **2018**, *18*, 7323.